

Phonon transmission and thermal conductance across graphene/Cu interface

Liang Chen,¹ Zhen Huang,² and Satish Kumar^{1,a)}

¹*G. W. Woodruff School of Mechanical Engineering, Georgia Institute of Technology, Atlanta, Georgia 30332, USA*

²*International Business Machine, Austin, Texas 78758, USA*

(Received 30 May 2013; accepted 30 August 2013; published online 18 September 2013)

We investigate phonon transmission and thermal boundary conductance (TBC) across graphene/Cu interface using density functional theory and atomistic Green's function method. The analysis of phonon dispersions and density of states of single layer graphene (SLG) shows that even weak SLG/Cu interaction can soften the transverse optical and longitudinal optical modes and suppress low frequency out-of-plane acoustic (ZA) modes. Our calculations predict that a small stretching of the SLG lattice ($\sim 1.6\%$) significantly enhances the SLG/Cu interaction which is reflected in larger band-gap for ZA/ZO phonon mode and a remarkable increase in TBC ($\sim 59\%$). © 2013 AIP Publishing LLC. [<http://dx.doi.org/10.1063/1.4821439>]

In graphene based electronic devices, thermal transport across graphene-metal interfaces becomes particularly important when contact resistance becomes an obstacle in the effective heat removal from the devices, e.g., at contacts in short channel field effect transistors (FETs) and graphene-Cu hybrid-interconnects.¹⁻³ The thermal boundary conductance (TBC) between graphene/graphite and various metals has been previously measured, and relatively low TBC at interfaces (e.g., 7–60 MW/m²K for graphene-Au⁴⁻⁶ and graphene-Cu⁷ at room temperature) has been reported. Low TBC at graphene interfaces^{8,9} can become a critical challenge for high frequency applications of graphene FETs and interconnects. Experimental measurements show that the TBC at graphene-metal interfaces has a weak dependence on temperature above 100 K.⁴ Phonons are, therefore, expected to be the dominant energy carriers for the interfacial thermal transport.⁴ Recently, the atomic and electronic structures of various graphene-metal interfaces have been investigated using density functional theory (DFT) calculations,¹⁰⁻¹⁴ but the predicted equilibrium spacing and binding energy have a large variation depending on the exchange-correlation functional and the lattice constant of graphene considered to match with the lattice of metal substrate. The equilibrium spacing between graphene and Cu substrate could vary from 2.24 Å to 3.58 Å depending on the lattice constants of graphene (2.44 Å to 2.55 Å) and exchange-correlation functional considered in the DFT calculations.¹⁰⁻¹⁵ The effects of these variations on the phonon transport across graphene-metal interfaces have not been studied.

In this letter, we study the phonon transmission and TBC across graphene/Cu interfaces using Atomistic Green's function (AGF)¹⁶⁻¹⁸ and DFT calculations. AGF based model compute the TBC across Cu/SLG/Cu interfaces using the atomic structure and interatomic force constants (IFCs) predicted from the DFT calculations. By comparing phonon dispersions of isolated graphene, Cu supported graphene, and graphene sandwiched between Cu layers, we find graphene-

Cu interaction can open a small gap between out-of-plane acoustic (ZA) and optical (ZO) modes at K point. The magnitude of this gap has indicated an enhanced graphene-Cu interaction in stretched graphene lattice compared to the unstretched graphene. We further show that this enhancement of graphene-Cu interaction due to the stretching of graphene lattice can significantly increase the phonon transmission and the TBC across the graphene-Cu interface. The prediction of TBC across SLG/Cu interface by AGF is in agreement with the previous experimental measurements,⁷ which suggests that our first principle method without using any adjustable parameters can serve as an efficient tool for the thermal analysis of graphene-metal interfaces.

We consider a single layer graphene (SLG) sandwiched between two Cu layers in the AGF calculations as shown in Fig. 1(a). At SLG/Cu interfaces, the SLG honeycomb lattice is positioned to match the Cu (111) lattice to form the top

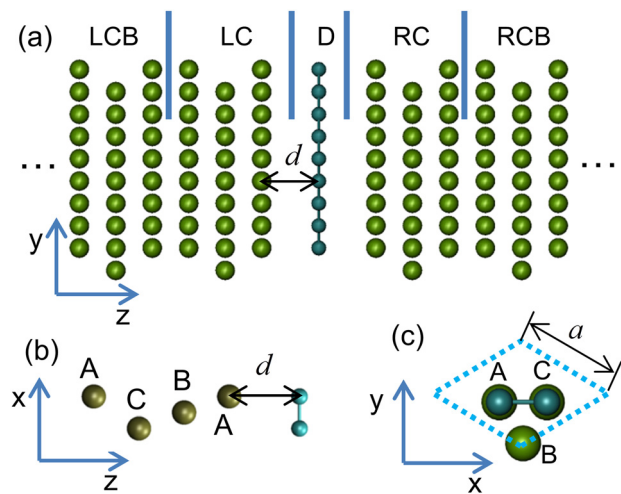


FIG. 1. (a) Schematic of Cu/SLG/Cu system for the AGF calculation. A single layer graphene (SLG) is considered as the device (D). It is sandwiched between two Cu contacts: left contact (LC) and right contact (RC). The regions beyond LC or RC are defined as the left contact bulk (LCB) and right contact bulk (RCB), which do not interact with the device region. View in (b) x-z plane and (c) x-y plane of a unit cell with 2 C atoms on Cu atoms. Only four layers of Cu are shown in (b).

^{a)}Author to whom correspondence should be addressed. Electronic mail: satish.kumar@me.gatech.edu.

TABLE I. Lattice constant (a) of unit cell shown in Fig. 1(c) and corresponding SLG-Cu equilibrium spacing (d).

	Case I	Case II
SLG lattice constant (\AA)	2.45	2.49
SLG-Cu spacing (\AA)	3.23	3.18

face-centered cubic (top-FCC) configuration (Fig. 1(b)), which is demonstrated to be the most stable configuration with lowest energy.^{11,14} In the absence of accurate empirical model to describe the graphene/Cu interactions, we employ DFT to determine the IFCs.

We first perform DFT simulations with local density approximation (LDA)¹⁹ functional to determine the optimized lattice constants of isolated SLG and bulk Cu, and equilibrium spacing d between SLG and Cu substrate, respectively. As shown in Fig. 1(c), we define the in-plane lattice constant of SLG/Cu system as length a which is also the definition of lattice constant of graphene primitive unit cell. The FCC lattice constant of bulk Cu is $a_{\text{FCC}} = \sqrt{2}a$. Here, we use a for the following discussion of bulk Cu, SLG, and SLG/Cu systems. The optimized lattice constants and equilibrium spacing are listed in Table I. We focus on the analysis of TBC and phonon interactions at graphene-Cu interface for two cases, which has different lattice constants for the unit cell in Fig. 1(c): Case I-graphene lattice constant determined by LDA, $a = 2.45 \text{\AA}$ and corresponding $d = 3.23 \text{\AA}$; Case II- Cu lattice constant determined by LDA, $a = 2.49 \text{\AA}$ and corresponding $d = 3.18 \text{\AA}$. In Case I, we optimize the SLG structure using LDA, and Cu lattice is compressed and matched to SLG lattice. In Case II, we obtain the optimized lattice constant of the Cu FCC structure using LDA, and SLG lattice is stretched to match the Cu lattice. The equilibrium spacing in Case II is reduced by 0.05\AA compared to Case I as the SLG lattice constant is increased from 2.45\AA in Case I to 2.49\AA in Case II. This indicates that the interaction between SLG and Cu can be enhanced by stretching the SLG lattice. The IFCs between C-C, Cu-Cu, and C-Cu atom pairs are determined using DFT calculations for the optimized lattice constants and equilibrium spacing (see supplemental material²⁰).

The phonon dispersion of SLG is determined by the diagonalizing the dynamical matrix constructed using IFCs obtained from the DFT simulations with LDA functional. Figure 2(a) compares the phonon dispersion of isolated SLG with unstretched lattice constant $a = 2.45 \text{\AA}$ and stretched lattice constant $a = 2.49 \text{\AA}$, and experimental measurements.²¹ As the lattice constant a is stretched by 1.6%, TO and LO modes are strongly softened by 3 THz for the entire Γ -K branch. The softening in LA modes increases from Γ point to K point with the largest softening of 2.3 THz at K point. The softening of LA, TO, and LO modes indicates the decrease of in-plane stretching force constant and increase of out-of-plane bending force constant due to the increase of C-C bond length.^{22,23} Compared to the experimentally measured dispersion relation of surface phonons of graphite in Fig. 2(a), the DFT calculation with unstretched lattice constant has a good agreement except for the ZA/ZO and LA/LO modes at K point. Our calculations show no splitting of the ZA/ZO modes and LA/LO modes at K point, but splitting of modes is observed in the experimental measurements.^{21,24} This disagreement might be because the thin flake of graphite used in the experiments^{24,25} had the possible admixture of microcrystallites of different orientations.²⁶

Figure 2(b) shows the phonon dispersions of Cu supported SLG (Fig. 1(c)) for unstretched graphene with lattice constant $a = 2.45 \text{\AA}$, stretched graphene with lattice constant $a = 2.49 \text{\AA}$, and experimental measurements.²¹ In the experiments by Shikin *et al.*,^{21,27} about one layer of Cu was intercalated underneath the SLG supported on Ni (111). In comparison to the phonon dispersion of isolated SLG in Fig. 2(a), TO and LO modes at Γ point are significantly softened, and ZO modes from Γ to K are slightly softened, which can be observed in both the DFT calculations and experimental measurements. The softening in TO, LO and ZO modes is because of the charge transfer from the d bands of Cu to C atoms in SLG which weakens the π bonding in SLG. The inset of Fig. 2(b) zooms in the region of green box which shows the ZA and ZO modes near K point. The slight splitting between ZA and ZO modes can be observed at K point. It is 0.05 THz for the unstretched SLG and 0.08 THz for the stretched SLG. Besides, a small lifting of acoustic modes is

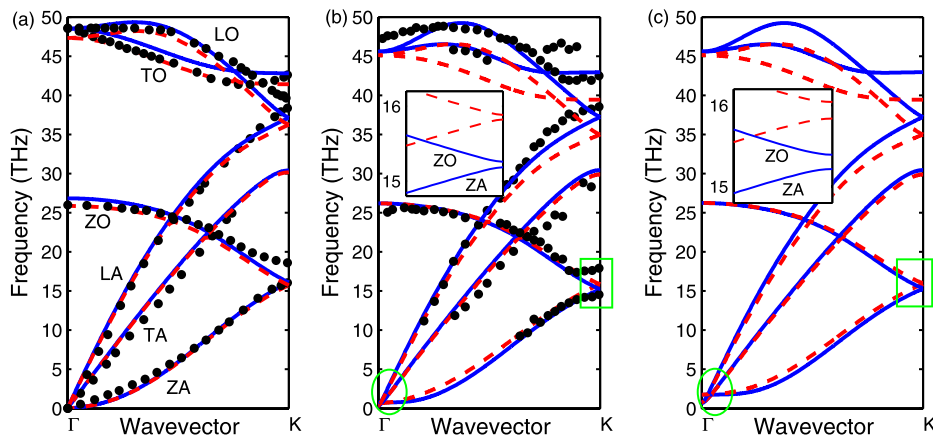


FIG. 2. Phonon dispersions of (a) isolated SLG; (b) SLG supported on Cu (111); (c) SLG sandwiched between two Cu (111) surfaces. Black dots in (a) and (b) are experimental measurements from Ref. 21 for surface phonons of pure graphite and phonon modes of graphene in graphene/Cu/Ni, respectively. Solid blue lines and red dashed lines in (a), (b) and (c) are calculated for the unstretched and stretched SLG, respectively. The insets in (b) and (c) are the zoom-in plot of ZA and ZO modes around K point as indicated by the green boxes. The lifting in ZA modes at Γ points is marked with green circles in (b) and (c).

observed at Γ point (e.g., 0.76 THz and 0.67 THz for ZA modes of the unstretched and stretched SLG), as indicated by the green circle in Fig. 2(b) and Fig. S1 in supplementary material.²⁰ When the SLG is sandwiched between the Cu layers, the gaps between ZA and ZO modes at K point are 0.17 THz and 0.2 THz for the two cases, respectively, as shown in Fig. 2(c). According to the previous studies,^{22,23} the gap between ZA and ZO modes at K points indicates the interaction strength between SLG and the metal substrate. The increase of the interaction strength can change the TBC, which will be demonstrated by AGF calculations.

The density of states (DOSs) of the lattices near the interface indicates the phonon population available for interfacial coupling over the frequency range of interest. We first compare the effect of SLG-Cu interactions on the density of states (DOSs) of Cu and SLG as shown in Figure 3. In left contact (LC) or right contact (RC) region, the strong Cu-Cu bonding at the SLG/Cu interface is replaced by weak interactions between Cu atoms and C atoms. This leads to a shift in Cu phonon DOSs to the lower frequencies (see in Fig. 3(a)). This frequency shift has also been observed in the DOSs of surface phonons in transition metals and silicon.^{28–30} The interaction with Cu substrate also affects the DOSs of graphene as shown in Fig. 3(b). The DOSs of graphene are

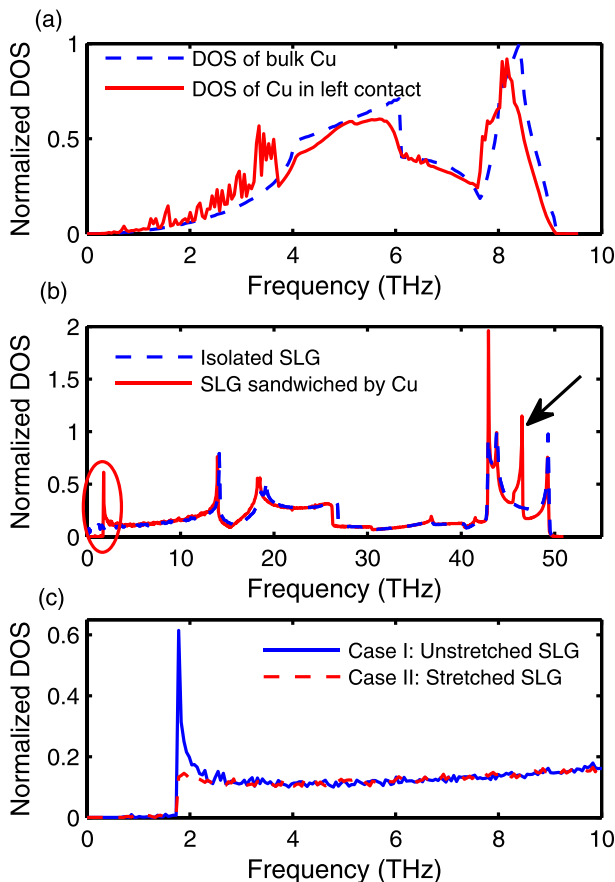


FIG. 3. (a) DOSs of bulk Cu and Cu in LC region of Cu/SLG/Cu system with unstretched SLG lattice constant. (b) DOSs of isolated SLG and SLG sandwiched between Cu layers of Cu/SLG/Cu system with unstretched SLG lattice constant. Region with suppressed ZA modes is marked with red circle while the new peak created by the softening of TO and LO modes is marked with black arrow. (c) DOSs of unstretched and stretched SLG in Cu/SLG/Cu system below 10 THz.

suppressed at low frequencies (<1.7 THz marked with red circle in Fig. 3(b)), while a new peak is observed around 46 THz (marked with black arrow in Fig. 3(b)) for the sandwiched SLG. The LO and TO modes are softened at frequencies around 46 THz (see Fig. 2(c)), and the abundance of these phonon modes around Γ point create the new peak in DOSs around 46 THz. Figure 3(c) compares the DOSs of device graphene for the two cases in low frequency region (0–10 THz). The DOSs of device graphene for Cases I and II are nearly zero below 1.8 THz, which corresponds to the lifting of ZA modes at Γ point in Fig. 2(c). At frequencies close to zero, the longitudinal acoustic (LA) and transverse acoustic (TA) phonon branches show linear relationship between frequency and wave vector, while the out-of-plane acoustic (ZA) phonon branch has a quadratic dispersion.³¹ DOSs of isolated graphene near zero frequency are populated by ZA modes.^{32,33} However, the DOSs of the device graphene decrease to almost zero at low frequency (<1.7 THz) which indicates that the ZA modes are highly suppressed at low frequency as shown in Fig. 3(c).³⁴

A distinct phonon spectrum mismatch between Cu and graphene can be observed by comparing Figs. 3(a) and 3(b). The phonon modes in Cu are below 9 THz, while the vibrational frequencies of graphene are up to 50 THz. This mismatch in phonon spectrum between graphene and Cu restricts the phonon transmission to the frequencies below 9 THz as shown in the inset of Fig. 4. By comparing transmission function with DOSs of SLG in Fig. 3(c), we observe that the behavior of phonon transmission at low frequency (below 1.7 THz) in each case is in agreement with the trends in DOSs of sandwiched SLG. The suppressed ZA modes below 1.7 THz cannot contribute to the phonon transmission across Cu/SLG/Cu interfaces. Figure 4 also shows the TBC as a function of temperature. Because the phonon transmission is generally limited to frequencies below 9 THz, the TBC levels off beyond 300 K. The TBC for Cases I and II is 10.4 MW/m²K and 16.5 MW/m²K at 300 K, respectively. The lattice constant of graphene is increased by 1.6%, and the

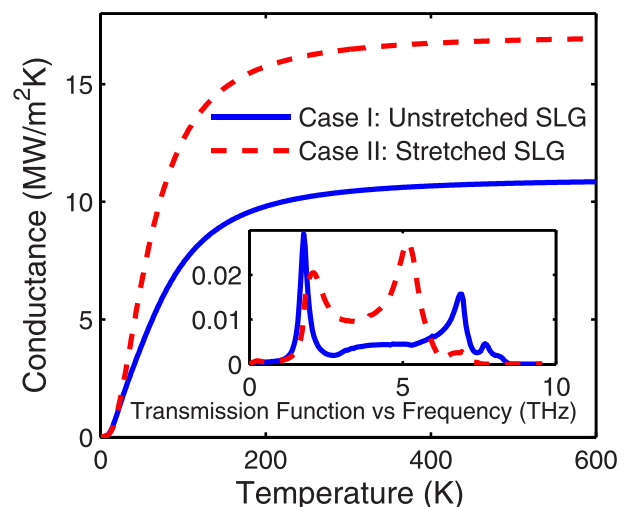


FIG. 4. Thermal boundary conductance at Cu/SLG/Cu interfaces as a function of temperature for unstretched and stretched SLG. The inset shows transmission function for the two cases.

equilibrium spacing is reduced by 1.5% from Case I to Case II (see Table I), but the TBC is increased by 59%. The interaction strength between SLG and Cu is increased in Case II compared to Case I, which is also in agreement with the phonon band gap increase between ZA and ZO modes at K point from Case I to II. As shown in the supplementary material,²⁰ TBC increases quadratically with the IFCs between SLG and Cu. A 26% increase of IFCs between SLG and Cu can lead to a 59% increase of TBC across Cu/SLG/Cu interfaces. As a result of stretching SLG lattice, the equilibrium spacing is reduced; the decrease in the equilibrium spacing enhances the interfacial interactions and therefore significantly increases the TBC.

The TBC shown in Fig. 4 corresponds to two Cu-graphene interfaces. Neglecting the thermal resistance across SLG,⁴ the TBC across single SLG/Cu interface at 300 K should be twice of the value shown in Fig. 4, i.e., 20.8 and 33 MW/m²K for Cases I and II. Experimental measurements have been reported for TBC across interface of highly ordered pyrolytic graphite (HOPG) and Cu.⁷ The as-cleaved sample had highest TBC of 60 MW/m²K, while the vacuum-cleaved sample yielded a lower TBC around 55 MW/m²K.⁷ The TBC for as-cleaved sample is higher because of the presence of absorbed impurities at interface which may have been introduced during the deposition of Cu on HOPG in the presence of the water and hydrocarbons.⁷ In this study, we use the crystalline Cu with smooth surface, and the calculated TBC (20.8 MW/m²K and 33.0 MW/m²K for unstretched and stretched cases, respectively) is lower but comparable to the experimental measurements. However, the higher TBC in the experimental measurements indicates stronger interaction between Cu and graphite which depends on the deposition technique and interface structure. The elevated temperature during the metal deposition can also increase the reactivity between metal and HOPG. Besides, the inelastic scattering at the interface, which is a challenge to include in the AGF calculation, can also contribute to the interfacial thermal transport. For materials with significant mismatch of phonon spectrum, the inelastic phonon scattering can open new channels for thermal transport.^{5,35-37}

In summary, we have investigated the effects of SLG and Cu lattice constants on the phonon transmission across Cu/SLG/Cu interfaces using AGF and DFT simulations. We demonstrate that the phonon DOSs of SLG and phonon transmission across SLG/Cu is nearly zero below 1.7 THz because of the suppression of ZA phonon modes in graphene. We find relatively low TBC (~10 to 16.5 MW/m²K) for all cases considered in this study, which can be attributed to the weak atomic interactions and significant mismatch of phonon spectrum. Stretching the SLG lattice to match Cu lattice reduces the spacing between SLG and Cu and enhances the interfacial interaction, which significantly increases the TBC (~by 59%).

This work was partially supported by National Science Foundation Grant CBET-1236416.

- ¹A. D. Liao, J. Z. Wu, X. R. Wang, K. Tahy, D. Jena, H. J. Dai, and E. Pop, *Phys. Rev. Lett.* **106**, 256801 (2011).
- ²F. Schwierz, *Nature Nanotechnol.* **5**, 487 (2010).
- ³T. H. Yu, C. W. Liang, C. Kim, E. S. Song, and B. Yu, *IEEE Electron Device Lett.* **32**, 1110 (2011).
- ⁴Y. K. Koh, M. H. Bae, D. G. Cahill, and E. Pop, *Nano Lett.* **10**, 4363 (2010).
- ⁵P. M. Norris, J. L. Smoyer, J. C. Duda, and P. E. Hopkins, *ASME Trans. J. Heat Transfer* **134**, 020910 (2012).
- ⁶A. J. Schmidt, K. C. Collins, A. J. Minnich, and G. Chen, *J. Appl. Phys.* **107**, 104907 (2010).
- ⁷J. J. Gengler, S. V. Shenogin, J. E. Bultman, A. K. Roy, A. A. Voevodin, and C. Muratore, *J. Appl. Phys.* **112**, 094904 (2012).
- ⁸A. K. Vallabhaneni, B. Qiu, J. N. Hu, Y. P. Chen, A. K. Roy, and X. L. Ruan, *J. Appl. Phys.* **113**, 064311 (2013).
- ⁹Z. Chen, W. Jang, W. Bao, C. N. Lau, and C. Dames, *Appl. Phys. Lett.* **95**, 161910 (2009).
- ¹⁰L. Adamska, Y. Lin, A. J. Ross, M. Batzill, and I. I. Oleynik, *Phys. Rev. B* **85**, 195443 (2012).
- ¹¹G. Giovannetti, P. A. Khomyakov, G. Brocks, V. M. Karpan, J. van den Brink, and P. J. Kelly, *Phys. Rev. Lett.* **101**, 026803 (2008).
- ¹²C. Gong, G. Lee, B. Shan, E. M. Vogel, R. M. Wallace, and K. Cho, *J. Appl. Phys.* **108**, 123711 (2010).
- ¹³Y. Matsuda, W. Q. Deng, and W. A. Goddard, *J. Phys. Chem. C* **111**, 11113 (2007).
- ¹⁴Z. P. Xu and M. J. Buehler, *J. Phys. Condens. Matter* **22**, 485301 (2010).
- ¹⁵M. Vanin, J. J. Mortensen, A. K. Kelkkanen, J. M. Garcia-Lastra, K. S. Thygesen, and K. W. Jacobsen, *Phys. Rev. B* **81**, 081408 (2010).
- ¹⁶N. Mingo and L. Yang, *Phys. Rev. B* **68**, 245406 (2003).
- ¹⁷W. Zhang, T. S. Fisher, and N. Mingo, *Numer. Heat Transfer, Part B* **51**, 333 (2007).
- ¹⁸A. Bulusu and D. G. Walker, *J. Appl. Phys.* **102**, 073713 (2007).
- ¹⁹J. P. Perdew and A. Zunger, *Phys. Rev. B* **23**, 5048 (1981).
- ²⁰See supplementary material at <http://dx.doi.org/10.1063/1.4821439> for parameters used in DFT and AGF calculations.
- ²¹A. M. Shikin, D. Farias, and K. H. Rieder, *Europhys. Lett.* **44**, 44 (1998).
- ²²T. Aizawa, R. Souda, S. Otani, Y. Ishizawa, and C. Oshima, *Phys. Rev. B* **42**, 11469 (1990).
- ²³A. Allard and L. Wirtz, *Nano Lett.* **10**, 4335 (2010).
- ²⁴S. Siebentritt, R. Pues, K. H. Rieder, and A. M. Shikin, *Phys. Rev. B* **55**, 7927 (1997).
- ²⁵H. Yanagisawa, T. Tanaka, Y. Ishida, M. Matsue, E. Rokuta, S. Otani, and C. Oshima, *Surf. Interface Anal.* **37**, 133 (2005).
- ²⁶L. Wirtz and A. Rubio, *Solid State Commun.* **131**, 141 (2004).
- ²⁷A. M. Shikin, V. K. Adamchuk, and K. H. Rieder, *Phys. Solid State* **51**, 2390 (2009).
- ²⁸F. Ducastel and F. Cyrotlac, *J. Phys. Chem. Solids* **31**, 1295 (1970).
- ²⁹F. Guinea, C. Tejedor, F. Flores, and E. Louis, *Phys. Rev. B* **28**, 4397 (1983).
- ³⁰J. Li, T. C. A. Yeung, and C. H. Kam, *J. Appl. Phys.* **111**, 094308 (2012).
- ³¹L. Lindsay and D. A. Broido, *Phys. Rev. B* **81**, 205441 (2010).
- ³²Z. Huang, T. S. Fisher, and J. Y. Murthy, *J. Appl. Phys.* **108**, 094319 (2010).
- ³³K. Saito, J. Nakamura, and A. Natori, *Phys. Rev. B* **76**, 115409 (2007).
- ³⁴J. H. Seol, I. Jo, A. L. Moore, L. Lindsay, Z. H. Aitken, M. T. Pettes, X. S. Li, Z. Yao, R. Huang, D. Broido, N. Mingo, R. S. Ruoff, and L. Shi, *Science* **328**, 213 (2010).
- ³⁵P. E. Hopkins, J. C. Duda, and P. M. Norris, *ASME Trans. J. Heat Transfer* **133**, 062401 (2011).
- ³⁶H. K. Lyo and D. G. Cahill, *Phys. Rev. B* **73**, 144301 (2006).
- ³⁷R. J. Stevens, L. V. Zhigilei, and P. M. Norris, *Int. J. Heat Mass Transfer* **50**, 3977 (2007).